

# Delayed triggering of microearthquakes by multiple surface waves circling the Earth

Zhigang Peng,<sup>1</sup> Chunquan Wu,<sup>1</sup> and Chastity Aiken<sup>1</sup>

Received 1 December 2010; revised 16 January 2011; accepted 24 January 2011; published 24 February 2011.

[1] It is well known that direct surface waves of large earthquakes are capable of triggering shallow earthquakes and deep tremor at long-range distances. However, it is not clear whether multiple surface waves circling the Earth could also trigger/modulate seismic activities. Here we conduct a systematic search of remotely triggered microearthquakes near the Coso Geothermal Field in central California following the 2010  $M_w$  8.8 Chile earthquake. We find a statistically significant increase of microearthquakes in the first few hours after the Chile mainshock. These observations of apparently delayed earthquake triggering do not follow the Omori-law decay with time since the largest  $M_L$  3.5 event occurred during the large-amplitude Love waves. Instead, they are better correlated with the first three groups of multiple surface waves ( $G_1 - R_1$ ,  $G_2 - R_2$ , and  $G_3$ ). Our observation provides an alternative explanation of delayed triggering of microearthquakes at long-range distances, at least in the first few hours after large earthquakes. **Citation:** Peng, Z., C. Wu, and C. Aiken (2011), Delayed triggering of microearthquakes by multiple surface waves circling the Earth, *Geophys. Res. Lett.*, *38*, L04306, doi:10.1029/2010GL046373.

## 1. Introduction

[2] Recent studies have shown that large earthquakes are capable of triggering microearthquakes and deep non-volcanic tremor at distances up to thousands of kilometers [Hill and Prejean, 2007; Peng and Gomberg, 2010, and references therein]. Many triggered seismic events occur instantaneously during the large-amplitude surface waves of distant earthquakes [Velasco et al., 2008; Peng et al., 2009; Wu et al., 2011], and are generally consistent with frictional failure on critically-stressed faults under the Coulomb failure criteria [Hill, 2008, 2010; Peng et al., 2010]. However, in some cases, elevated seismicity continues long after the passage of the surface waves, and the mechanism of such delayed triggering is still unclear [Hill and Prejean, 2007]. Some have invoked redistribution of pore fluids [Brodsky and Prejean, 2005], altered frictional contacts within fault zones [Parsons, 2005], or triggered aseismic creep events [Shelly et al., 2011], while others suggested that they are simply aftershocks of the instantaneously triggered events [Brodsky, 2006].

[3] Due to the finiteness of the Earth, surface waves produced by large earthquakes can circle the globe many times [e.g., Stein and Wysession, 2003]. They are denoted as

$G_n$  for Love waves, and  $R_n$  for Rayleigh waves. The index  $n$  denotes the time taken to circle the Earth, with the odd number ( $G_1$ ,  $G_3$ , etc) corresponding to the shortest path between the source and receiver and the even number ( $G_2$ ,  $G_4$ , etc) denoting the opposite path. Figure S1 of the auxiliary material shows the record sections for vertical displacement seismograms generated by the  $M_w$  8.8 earthquake that occurred offshore Maule, Chile on 2010/02/27.<sup>1</sup> The  $R_1$  to  $R_4$  Rayleigh waves are clearly visible, and have peak amplitudes on the order of a few fraction of a centimeter. The associated peak ground velocities for the multiple surface waves is on the order of 0.01 cm/s, which corresponds to a dynamic stress of  $\sim 1$  kPa (assuming a nominal phase velocity of 4 km/s and shear rigidity of 40 GPa). These numbers are close to the apparent triggering threshold of a few kPa found from recent systematic studies of triggered microearthquakes and tremor around the world [Brodsky and Prejean, 2005; Peng et al., 2009; Aiken et al., 2010; K. Chao et al., Remote triggering of non-volcanic tremor around Taiwan, submitted to *Geophysical Journal International*, 2010], suggesting that the later arriving multiple surface waves could have the potential of triggering/modulating microearthquakes.

[4] To test this hypothesis, we examine the continuous seismic recordings near the Coso Geothermal Field (CGF) in central California (Figure 1)  $\sim 12$  hours before and after the 2010  $M_w$  8.8 Chile earthquake. We choose this region mainly because it is one of the most seismically active regions in California [Bhattacharyya and Lees, 2002], and is repeatedly triggered by large regional and teleseismic earthquakes [e.g., Prejean et al., 2004; Aiken et al., 2010]. In particular, Peng et al. [2010] found 4  $M_L \geq 2$  events listed in the Southern California Seismic Network (SCSN) catalog during the passage of the teleseismic waves of the 2010 Chile mainshock, including an  $M_L$  3.5 event that coincides with the 200-s mantle Love wave. In this work, we extend our previous study by manually picking local earthquakes from band-pass filtered seismograms in a longer time frame and examining the correlations with the multiple surface waves produced by the 2010 Chile mainshock.

## 2. Analysis Procedure

[5] The analysis procedure generally follows that of Peng et al. [2007] and is briefly described here. We use the continuous three-component seismograms recorded by the broadband station JRC2 in the CGF in this study. We first remove the instrument response, integrate into displacement, demean and detrend the displacement data, and then apply a two-pass 4th-order 2–16 Hz Butterworth filter to remove

<sup>1</sup>School of Earth and Atmospheric Sciences, Georgia Institute of Technology, Atlanta, Georgia, USA.

<sup>1</sup>Auxiliary materials are available in the HTML. doi:10.1029/2010GL046373.

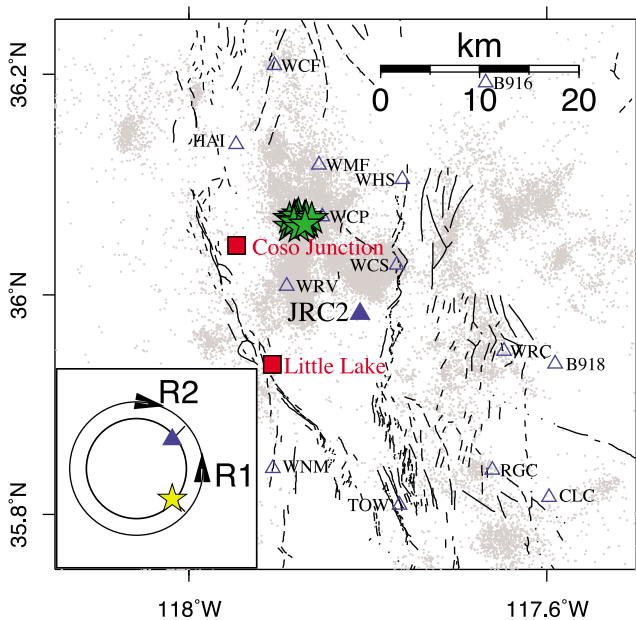


**Figure 1.** Map view of the study region around the Coso Geothermal Field in central California. Seismic stations belonging to the Southern California Seismic Network (SCSN) are denoted as blue triangles. Gray dots signify earthquakes since 1999 listed in the SCSN catalog. The earthquake catalogs are downloaded from Southern California Earthquake Data Center (SCEDC) within a rectangular area (longitudes between  $-118.25^\circ$  and  $-117.5^\circ$ , and latitudes between  $35.75^\circ$  and  $36.25^\circ$ ) that bounds our study region. Green stars represent 15 earthquakes that occurred 12 hours before and after the 2010  $M_w$  8.8 Chile main shock. The inset shows a cartoon illustrating the multiple surface waves circling the Earth from the source (yellow star) to receiver (blue triangle).

long-period teleseismic signals. We compute the envelopes of the band-pass filtered seismograms, smooth the envelope by a mean operator with a half width of 50 data points (0.5 s), and finally stack the three-component envelopes. Next, we identify earthquakes as high-frequency impulsive seismic energy in the 2–16 Hz band-pass filtered seismograms and double picks in the envelope that correspond to the  $P$  and  $S$  arrivals. To ensure that the identified events are of local origin, we require that the  $S - P$  time for each event is less than 5 s, which roughly corresponds to the epicentral distance of  $\sim 40$  km. Next, we find the peak amplitude for each event and use the time corresponding to the peak amplitude as a proxy for the event origin time, as was done by Peng *et al.* [2007]. The actual origin time would be a few seconds earlier, but such a difference is negligible in the following analysis. Overall, we have identified a total of 116 events (Figure 2a) within 12 hour before and after the theoretical  $P$  arrival of the Chile mainshock (742.4 s after the origin time 2010/02/27, 06:34:14 UTC), as predicted by the iasp91 model [Kennett and Engdahl, 1991].

[6] It is well known that a ten-fold increase in amplitude generally corresponds to one unit increase in magnitude. Therefore, the measured peak amplitudes of the 116 manually picked events provide good estimation for their magnitudes. Figure 2b shows the magnitude–amplitude relationship for 15 events that are also listed in the SCSN

catalog. The magnitudes and  $\log_{10}(\text{amplitudes})$  follow the 1–1 slope, and the best fitting relationship is  $M = 0.977 \times \log_{10}(A) + 6.32$ , where  $M$  is the inferred magnitude, and  $A$  is the peak displacement in cm. We use this relationship to convert the peak displacements of all events into magnitudes, without considering the effects of epicentral distances. The median value of the  $\log_{10}$  envelope function is  $-7.32$ , which roughly corresponds to the inferred magnitude  $-0.83$ , denoting the smallest possible events we can identify from this procedure. The manually picked events generally follow the Gutenberg–Richter frequency–size relationship, but the corresponding  $b$ -values (Figure 2c) from both least-squares fitting and maximum-likelihood estimates are very low ( $< 0.5$ ). These numbers, however, are marginally within the 1-standard deviations of the  $b$ -values estimated directly from the events listed in the SCSN catalog around the occurrence time of the Chile mainshock (Figure S2), suggesting that the low  $b$ -value found in this study is not purely an artifact of misidentification of smaller events. The magnitude of completeness  $M_c$  value, which is the largest magnitude between those determined from the maximum curvature (MAXC) and the goodness-of-fit (GOF) methods [Wiemer and Wyss, 2000], is  $-0.4$ . We only use 99 events with  $M \geq M_c$  value in the subsequent analysis.

### 3. Relationship Between Local Events and Multiple Surface Waves

[7] Figure 3 shows a comparison of the envelope functions, manually picked events, and the displacement seismograms recorded at station JRC2 around the Chile mainshock. The time windows associated with the group

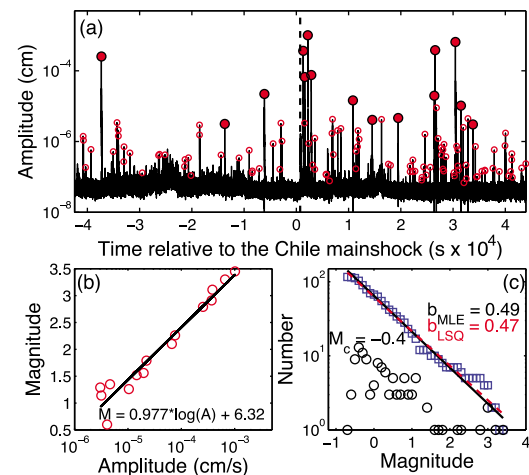


**Figure 2.** (a) The 2–16 Hz band-pass filtered envelope function at station JRC2 showing manually picked local earthquakes (open circles) 12 hours before and after the 2010  $M_w$  8.8 Chile mainshock. The large solid circles mark the events that are also listed in the SCSN catalog. The vertical dashed line marks the predicted  $P$  arrival. (b) The magnitudes for 15 events that are listed in the catalog versus their peak amplitudes. The dark line marks the least-squares fitting of the data. (c) Cumulative (blue square) and discrete (black circle) frequency-magnitude distributions for all the hand-picked events. The black solid and red dashed lines mark the  $b$ -value fit from least-squares and maximum-likelihood methods, respectively.

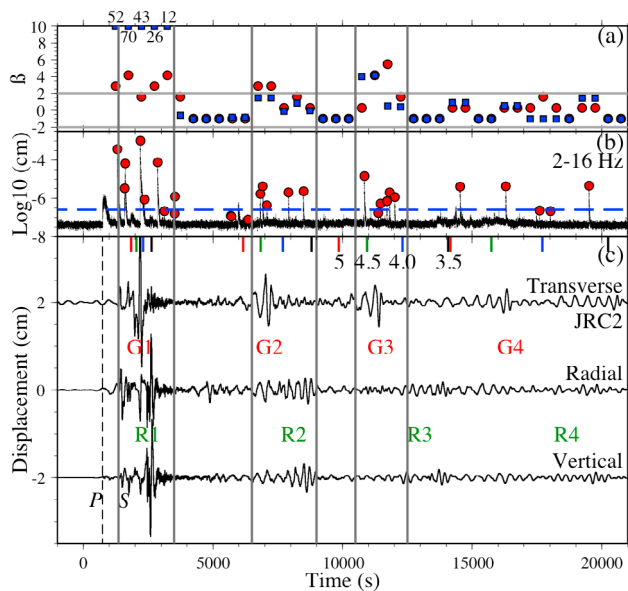


**Figure 3.** (a) The sliding-window  $\beta$ -values measured from all manually picked events (red circles) above the magnitude of completeness  $M_c = -0.4$  and envelope functions (blue squares) after the Chile main shock. The horizontal gray lines mark the  $\beta$ -values of  $\pm 2$ . The  $\beta$ -values for the envelope functions are clipped at 10 (with true values marked) for plotting purpose. The vertical gray lines correspond to the time windows that show statistically significant triggering (i.e.,  $\beta$ -value  $> 2$ ). (b) The 2–16 Hz band-pass filtered envelope function showing local earthquakes (red circles) around Coso. The blue dashed line marks the 9 times the Median Absolute Deviation (MAD). (c) The instrument-corrected three-component displacement seismograms showing the teleseismic body waves, and multiple-surface waves generated by the 2010 Chile mainshock. The vertical dashed line marks the predicted arrival of the  $P$  wave. The short red, green, blue and black lines on the top mark the arrival times that correspond to the group velocities of 5, 4.5, 4, and 3.5 km/s.

velocities of 4–5 km/s and 3.5–4.5 km/s roughly correspond to the arrivals of the  $G_n$  and  $R_n$  waves, respectively. We find that nine events occurred between the teleseismic  $S$  wave and immediately after the  $G_1$  and  $R_1$  waves ( $\sim 1300$ – $\sim 3500$  s, with 4 listed in the SCSN catalog), as reported by Peng *et al.* [2010]. This is followed by a relative quiescence between  $\sim 3500$  and  $\sim 5600$  s. There is a strong burst of activity between  $\sim 5600$  and  $\sim 7500$  s during the  $G_2$  waves, and two earthquakes during the subsequent  $R_2$  waves between  $\sim 7500$  and  $\sim 9000$  s. Following these events, there is another brief period of quiescence, and then a strong burst of activity during and immediately after the  $G_3$  waves between  $\sim 10500$  and  $\sim 12500$  s. No clear seismic activity is observed during the  $R_3$  waves (i.e., from  $\sim 12500$  to  $\sim 14000$  s). After that, we could not identify any further correlations with the subsequent  $G_n$  and  $R_n$  waves. A swarm-like activity occurred about  $\sim 27000$  s after the mainshock and does not appear to have any correlations with the teleseismic surface waves (Figure 2).

[8] To further quantify the relationship between the manually picked events and multiple surface waves, we

perform two types of statistical analysis. First, we compare the seismicity rate immediately before and after the  $P$  wave of the Chile main shock and compute the  $\beta$ -statistic value [e.g., Kilb *et al.*, 2002], which is a measure of the difference between the observed number of events after the main shock and the expected number from the averaged rate before the main shock. The  $\beta$ -value for all the events is 3.4, while the  $\beta$ -value for events above the  $M_c$  value is 2.4. Both numbers are slightly above 2, suggesting that there is a moderate increase of seismic activity near Coso following the Chile main shock.

[9] Next, we compute the  $\beta$ -value using a small time window of 1000 s, and slide every 500 s after the teleseismic  $P$  waves. The choice of the window length is somewhat subjective, which reflects a compromise between a long-enough window for stable measurements and short-enough window for detailed information. The results from this and other choices of time windows ranging from 500, 2000, to 3000 s (Figure S3) show that the  $\beta$ -values generally track the number of events and are above 2 during the first three groups of the multiple surface waves, suggesting a statistically significant triggering. The  $\beta$ -value during the  $G_4$  and  $R_4$  waves is less than 2, and hence the apparent triggering is not well established. In addition, the expected  $\beta$ -value outside the multiple surface wave periods is  $-1.02$  when no events occur (Figure S3).

[10] In the second method, we directly measure the  $\beta$ -value from the band-pass filtered envelope functions [Jiang *et al.*, 2010] by summing the  $\log_{10}$  amplitudes in different time periods that are above 9 times the maximum absolute deviation (MAD) of the envelope functions (i.e., above

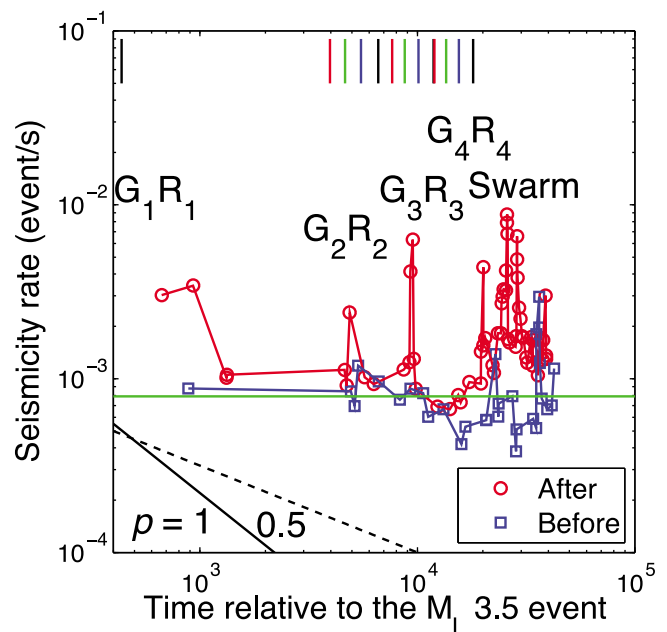


**Figure 4.** Seismicity rate before (blue) and after (red) the  $M_L$  3.5 earthquake that occurred during the large-amplitude Love wave. The horizontal green line marks the average rate before the  $M_L$  3.5 earthquake, and the solid and dashed lines show the reference Omori's law decay rate with  $p = 1$  and 0.5, respectively. The short red, green, blue and black lines on the top mark the arrival times that correspond to the group velocities of 5, 4.5, 4, and 3.5 km/s.

−6.6, or inferred magnitude of −0.13). The resulting  $\beta$ -values (Figure 3a) show similar patterns, although the fluctuations are much larger due to the heavy weight towards large-magnitude events. Nevertheless, it is evident from both approaches that there is an apparent correlation between the multiple surface waves of the Chile earthquake and the local seismicity near Coso, at least for the first three groups.

[11] The largest magnitude earthquake during our study period is an  $M_L$  3.5 event that occurred during the large-amplitude Love wave [Peng *et al.*, 2010]. To check if the subsequent events could simply be aftershocks of this event [Brodsky, 2006], we compute the seismicity rate relative to this  $M_L$  3.5 based on a sliding window technique with a fixed data window of 5 events [Peng *et al.*, 2007]. Figure 4 shows that while the events during the  $G_1$  and  $R_1$  waves could be considered as aftershocks of the  $M_L$  3.5 event (however, with only 3 data points, it is not clear), the events occurred during the subsequent multiple surface waves and the swarm period do not follow the Omori law decay. Hence, these events could not be simply explained as aftershocks of the directly triggered events.

#### 4. Discussions

[12] In this short note we showed that multiple surface waves from the 2010  $M_w$  8.8 Chile earthquake trigger/modulate microearthquake activity at the CGF in central California. To our knowledge, this is the first evidence of earthquake triggering by multiple surface waves, in addition to the abundant observations of triggering from the direct  $G_1$  and  $R_1$  waves [e.g., Hill and Prejean, 2007]. A few studies in the past have focused on the potentials for free oscillations of the Earth to trigger foreshocks [Costello and Tullis, 1999] or aftershocks [Kamal and Mansinha, 1996], and the results were not consistent. These studies might be relevant to our work if multiple surface waves could be considered as specific modes of free oscillations [e.g., Stein and Wysession, 2003].

[13] Our observations (e.g., Figure 4) suggested that the microearthquake activity in the first few hours at CGF did not follow an Omori's law decay with time since the direct surface waves of the 2010 Chile main shock (i.e., the  $G_1$  and  $R_1$  waves). Instead, their occurrence times match well with the arrivals of the multiple surface waves circling the Earth (Figure 3). This provides an alternative explanation for the delayed triggering at long-range distances, at least in the first few groups of the multiple surface waves ( $G_1 - R_1$ ,  $G_2 - R_2$ , and  $G_3$ ). In this case, the time delay is produced by the propagation of multiple surface waves, rather than at the triggered site as previous models have suggested [Brodsky and Prejean, 2005; Parsons, 2005; Brodsky, 2006; Shelly *et al.*, 2011].

[14] It is worth noting that such effects would probably only work for very large earthquakes (e.g.,  $M_w \geq 8.0$ ) that are capable of producing multiple surface waves circling the Earth with large-enough amplitudes. Hence, it cannot be applied to explain all observations of delayed triggering. In addition, the triggering effects from multiple surface waves would be most apparent in the first few groups because of the decaying amplitudes and dispersion (Figure 3). The peak displacement and velocity measured during the  $G_3$  waves are  $\sim 0.56$  cm and 0.017 cm/s, respectively, which corre-

sponds to a dynamic stress of 1.7 kPa. This value is close to the aforementioned triggering thresholds for tremor and microearthquakes found elsewhere [Peng *et al.*, 2009; Aiken *et al.*, 2010; Chao *et al.*, submitted manuscript, 2010], suggesting that the lack of triggering by later arriving surface waves could be due to their small amplitudes.

[15] An interesting distance range for observing triggering by multiple surface waves is at  $180^\circ$  (antipodal distance) or  $360^\circ$  (epicenter). Because the surface wave amplitudes are larger at these distance ranges due to a superposition effect (e.g., Figure S1), we would expect to see higher potential of triggering by multiple surface waves. Recently, Lin [2010] found that one of the large aftershocks of the 2008  $M_w$  7.9 Wenchuan earthquake occurred during the large-amplitude  $ScS$  wave, and proposed that teleseismic waves returning back to the epicentral region could modulate aftershock activity. It remains to be tested whether the multiple surface waves returning back to the epicentral region have the same potential of triggering additional aftershocks. This is an interesting subject that will be analyzed in a follow-up study.

[16] **Acknowledgments.** The seismic data and earthquake catalog used in this study are downloaded from the Southern California Earthquake Data Center (SCEDC). We thank Aaron Velasco, an anonymous reviewer, and the editor Ruth A. Harris for their useful comments. This study was supported by the National Science Foundation through award EAR-0956051.

#### References

- Aiken, C., Z. Peng, and C. Wu (2010), Dynamic triggering of microearthquakes in the Long Valley Caldera and Coso Geothermal Field, *Eos Trans. AGU*, 91, Fall Meet. Suppl., Abstract S33B-2103.
- Bhattacharyya, J., and J. M. Lees (2002), Seismicity and seismic stress in the Coso Range, Coso geothermal field, and Indian Wells Valley region, southeast-central California, in *Geologic Evolution of the Mojave Desert and Southwestern Basin and Range*, edited by A. F. Glazner, J. D. Walker, and J. M. Bartley, *Geol. Soc. Am. Mem.*, 195, 243–257.
- Brodsky, E. E. (2006), Long-range triggered earthquakes that continue after the wave train passes, *Geophys. Res. Lett.*, 33, L15313, doi:10.1029/2006GL026605.
- Brodsky, E. E., and S. G. Prejean (2005), New constraints on mechanisms of remotely triggered seismicity at Long Valley Caldera, *J. Geophys. Res.*, 110, B04302, doi:10.1029/2004JB003211.
- Costello, S., and T. E. Tullis (1999), Can free oscillations trigger foreshocks that allow earthquake prediction?, *Geophys. Res. Lett.*, 26, 891–894, doi:10.1029/1999GL900143.
- Hill, D. P. (2008), Dynamic stresses, coulomb failure, and remote triggering, *Bull. Seismol. Soc. Am.*, 98, 66–92, doi:10.1785/0120070049.
- Hill, D. P. (2010), Surface wave potential for triggering tectonic (non-volcanic) tremor, *Bull. Seismol. Soc. Am.*, 100, 1859–1878, doi:10.1785/0120090362.
- Hill, D. P., and S. G. Prejean (2007), Dynamic triggering, in *Treatise on Geophysics*, vol. 4, *Earthquake Seismology*, edited by G. Schubert and H. Kanamori, pp. 257–292, Elsevier, Amsterdam.
- Jiang, T., Z. Peng, W. Wang, and Q.-F. Chen (2010), Remotely triggered seismicity in continental China by the 2008 Mw7.9 Wenchuan earthquake, *Bull. Seismol. Soc. Am.*, 100, 2574–2589, doi:10.1785/0120090286.
- Kamal, X., and L. Mansinha (1996), The triggering of aftershocks by the free oscillations of the Earth, *Bull. Seismol. Soc. Am.*, 86, 299–305.
- Kennett, B. L. N., and E. R. Engdahl (1991), Traveltimes for global earthquake location and phase identification, *Geophys. J. Int.*, 105, 429–465, doi:10.1111/j.1365-246X.1991.tb06724.x.
- Kilb, D., J. Gomberg, and P. Bodin (2002), Aftershock triggering by complete Coulomb stress changes, *J. Geophys. Res.*, 107(B4), 2060, doi:10.1029/2001JB000202.
- Lin, C.-H. (2010), A large Mw 6.0 aftershock of the 2008 Mw 7.9 Wenchuan earthquake triggered by shear waves reflected from the Earth's core, *Bull. Seismol. Soc. Am.*, 100, 2858–2865, doi:10.1785/0120090141.

- Parsons, T. (2005), A hypothesis for delayed dynamic earthquake triggering, *Geophys. Res. Lett.*, *32*, L04302, doi:10.1029/2004GL021811.
- Peng, Z., and J. Gomberg (2010), An integrated perspective of the continuum between earthquakes and slow-slip phenomena, *Nat. Geosci.*, *3*, 599–607, doi:10.1038/ngeo940.
- Peng, Z., J. E. Vidale, M. Ishii, and A. Helmstetter (2007), Seismicity rate immediately before and after main shock rupture from high-frequency waveforms in Japan, *J. Geophys. Res.*, *112*, B03306, doi:10.1029/2006JB004386.
- Peng, Z., J. E. Vidale, A. G. Wech, R. M. Nadeau, and K. C. Creager (2009), Remote triggering of tremor along the San Andreas Fault in central California, *J. Geophys. Res.*, *114*, B00A06, doi:10.1029/2008JB006049.
- Peng, Z., D. P. Hill, D. R. Shelly, and C. Aiken (2010), Remotely triggered microearthquakes and tremor in central California following the 2010  $M_w$  8.8 Chile earthquake, *Geophys. Res. Lett.*, *37*, L24312, doi:10.1029/2010GL045462.
- Prejean, S. G., D. P. Hill, E. E. Brodsky, S. E. Hough, M. H. S. Johnston, S. D. Malone, D. H. Oppenheimer, A. M. Pitt, and K. B. Richards-Dinger (2004), Remotely triggered seismicity on the United States west coast following the M 7.9 Denali fault earthquake, *Bull. Seismol. Soc. Am.*, *94*, S348–S359, doi:10.1785/0120040610.
- Shelly, D. R., Z. Peng, D. P. Hill, and C. Aiken (2011), Tremor, triggered creep, and the potential for delayed dynamic earthquake triggering, *Nat. Geosci.*, in press.
- Stein, S., and M. Wysession (2003), *An Introduction to Seismology, Earthquakes, and Earth Structure*, Blackwell, Malden, Mass.
- Velasco, A. A., S. Hernandez, T. Parsons, and K. Pankow (2008), Global ubiquity of dynamic earthquake triggering, *Nat. Geosci.*, *1*, 375–379, doi:10.1038/ngeo204.
- Wiemer, S., and M. Wyss (2000), Minimum magnitude of completeness in earthquake catalogues: examples from Alaska, the western United States, and Japan, *Bull. Seismol. Soc. Am.*, *90*, 859–869, doi:10.1785/0119990114.
- Wu, C., Z. Peng, W. Wang, and Q.-F. Chen (2011), Dynamic triggering of shallow earthquakes near Beijing, China, *Geophys. J. Int.*, in press.
- C. Aiken, Z. Peng, and C. Wu, School of Earth and Atmospheric Sciences, Georgia Institute of Technology, 311 Ferst Dr., Atlanta, GA 30332, USA. (zpeng@gatech.edu)